Supporting Information

Nitrogen-doped Carbon Fibers Embedding CoO_x Nanoframes Towards Wearable Energy Storage

Cheng Yang[a,b], Yuzhu Li[a,b], Binbin Zhang[a,b], Yuebin Lian[a,b], Yong Ma[a,b], Xiaohui Zhao[a,b], Xiangqiong Zeng[c], Jiusheng Li[c], Zhao Deng*[a,b], Jing Ye[d], Wenbin Wu[e], Yang Peng*[a,b]

[a] *Soochow Institute for Energy and Materials Innovations, College of Energy, Soochow University, Suzhou, 215006, China*

[b] *Jiangsu Provincial Key Laboratory for Advanced Carbon Materials and Wearable Energy Technologies, Soochow University, Suzhou, 215006, China*

[c] *Laboratory for Adanced Lubricating Materials, Shanghai Advanded Research Institute, Chinese Academy of Science, Shanghai 201210, China*

[d] *Analysis and Testing Center, Soochow University, Suzhou 215123, China*

[e] *KeTai Advanced Materials Co., Ltd. Jiangxi, China*

*Corresponding authors.

Tel: +86-512-6716-7407; E-mail: ypeng@suda.edu.cn (Y. Peng),

zdeng@suda.edu.cn (Z. Deng)

Experimental

1. Chemicals

All chemicals, $Co(NO_3)_2•6H_2O$ (Sinopharm Chemical Reagent Co., Ltd, China), CH_3OH (Sinopharm Chemical Reagent Co., Ltd, China), 2-methylimidazole ($C_4H_6N_2$) (98%, Aladding, China), N,N-dimethylformamide (DMF) (≥99.5%, Greagent, China), polyacrylonitrile (PAN) (Mw 200,000, Polysciences, USA) were used as obtained without further purification. Commercial Pt/C (20 wt%) was purchased from Johnson Matthey, and RuO_2 was purchased from Sigma-Aldrich.

2. Synthesis of ZIF-67

ZIF-67 was prepared through the method reported previously with a slight modification. Firstly, 4.65 g of $Co(NO_3)_2•6H_2O$ was dissolved in 200 mL of methanol to obtain solution A. Next, 4.926 g of 2-methylimidazole was dissolved in 200 mL methanol to prepare solution B. Then, solution B was added to solution A forming a homogeneous mixture. The mixture was stirred for 20 min, and then rested for 12h. Finally, the obtained powder was washed with methanol three times and vacuum dried at 60 °C for 12 h.

3. Synthesis of CoO_x@NC

First of all, 0.5 g PAN was added into 8.5 g DMF. The mixture was stirred at 50 °C to obtain a pale yellow clear solution. After cooling down 1g ZIF-67 was dispersed into the above solution, and the dispersion was then loaded into a plastic syringe with a stainless steel needle. The electrospinning process was carried at 17 kV between the needle and collector (10 cm apart) and a flow rate of 13 uL min^{-1}. Afterwards, the collected film was dried at 60 °C overnight. In order to obtain a robust and flexible film after carbonization, the as-spun film was preheated at a ramping rate of 2.5 °C

min^{-1} to 260 °C, and kept for 100 min in air. Subsequently, the pre-oxidized film was carbonized at 600 °C with a temperature-ramping rate of 3 °C min^{-1}, and kept for 100 min under Ar atmosphere in a tube furnace. Accordingly, the thus prepared films were designated as CoO_x@NC-600. Similarly, CoO_x@NC-700, CoO_x@NC-800 and CoO_x@NC-900 were prepared in the same way except under different carbonization temperature. For reference studies, ZIF-67 particles and pure PAN fibers were pre-oxidized and then carbonized following the same procedure of preparing CoOx@NC-600 to obtain the control samples of calcined ZIF-67 and carbonized PAN.

4. Material characterizations

Surface morphology and microstructural characterizations were performed by a field-emission scanning electron microscope (FE-SEM, Hitachi SU8010) and a high-resolution transmission electron microscope (HR-TEM, FEI Tecnai F20 200 kV). The chemical states of surface elements in the composite fibers were probed by X-ray photoelectron spectroscopy (XPS, ESCALAB 250Xi) using a Monochromatic Al Kα (1486.6 eV) X-ray source. X-ray diffraction (XRD, Bruker D8 Advance) was used to determine the crystalline structure of the carbonized fibers, and Raman spectra were obtained using a LabRAM HR Evolution Spectrometer. Thermal gravimetric analysis (TGA) was performed with EXSTAR 7300 under air with a heating rate of 10 °C min^{-1}. Brunauer-Emmett-Teller method (BET, Micromeritics ASAP2020) was applied to test the porosity of films with the Barrett-Joyner-Halenda (BJH) method adopted to determine the specific surface area and pore structure of the composites. Inductively coupled plasma emission spectrometer (ICP, PerkinElmer OPTIMA 8000) was used to determined the content of Co in the composites and the electric conductivity of samples was measured by a ST2263 dual-mode digital four-probe tester. 2.5. 5.Assembly and testing of Sodium-ion batteries

CoO_x@NC composite films were pouched into dia. 1.0 cm discs with mass loadings of 1 - 2 mg cm^{-2}, which were directly used as binder-free anodes. For control studies, the calcined ZIF-67 nanoparticles were used for preparing conventional anodes by casting a mixture of the active materials, Super P, and binder (polyvinylidene fluoride, PVDF) in a weight ratio of 60: 20: 20 onto the copper foil. The electrochemical performance of the as-fabricated working electrodes was examined using CR2025 coin-type half cells with 1 M $NaClO_4$ in a mixture of ethylene carbonate (EC) and diethylcarbonate (DEC) (1 : 1, by volume) containing 5 vol% fluoroethylene carbonate (FEC) as the electrolyte, sodium foil as the counter electrode and glass fiber as the separator. The electrochemical performance of the assembled cells was tested by using a battery test system (LANHE CT2100A, Wuhan electronics Co., China) in the voltage range from 0.01 to 3.0 V vs. Na/Na^+. Electrochemical impedance spectra (EIS) were collected over the frequency range from 0.01 Hz to 100 kHz on an electrochemical workstation (CHI-760E). Cyclic voltammetry (CV) was performed at a scan rate of 0.1 mV s^{-1} within the potential range of 0.01–3.0 V. For the fabrication of flexible SIB full cells, thin film cathodes synthesized by electrospinning 1g $Na_3V_2(PO4)_3$ and 1 g PAN in 12 g DMF, and followed by annealing at 600 °C in Ar for 2 h, were cropped into the same size as the CoO_x@NC-600 anode. The mass ratio of CoO_x@NC-600 to $Na_3V_2(PO_4)_3$ was controlled at about 1:5 to balance the capacity. The testing voltage window was optimized to be 0.01-3 V. The as-assembled CoO_x@NC-600-$Na_3V_2(PO4)_3$ full batteries were first activated at a relatively low current density of 100 mA g^{-1} for 3 cycles, and then charged/discharged at 500 mA g^{-1} for 200 cycles (current density based on the mass of anodic CoO_x@NC-600).2.6. 6.Electrocatalytic ORR and OER

For ORR: Electrocatalytic measurements were performed in a three-electrode system with 0.1 M KOH as the electrolyte. A glass carbon rotating disk electrode (RDE, diameter 5 mm), a saturated KCl Ag/AgCl electrode, and a carbon rod were used as the working electrode, reference electrode and counter electrode, respectively. All LSV data were obtained with 100% ir-correction, and all the potentials were calibrated to RHE according to the equation $E_{RHE} = E_{Ag/AgCl} + 0.059\ pH + 0.198\ V$. The catalyst ink was prepared by dispersing 4 mg active material and 2 mg Ketchen Black in a mixed solution of 0.2 mL ethanol, 0.8 ml water, and 0.02 mL Nafion (5 wt%), ultrasonicated for 2 h. Then 20 μL of the catalyst ink was pipetted onto the GC surface, accounting for an actual catalyst loading of 0.37 mg cm^{-2}. Before taking linear sweep voltammetry (LSV), O_2 was flowed into the reaction cell for 20 min, followed by 100 cycles of cyclic voltammetry (CV) scans. The scan rate of CV was 100 mV s^{-1} with a potential range from 1.1 V to 0.2 V (*vs.* RHE). The LSV was obtained with a scan rate of 10 mV/s with the rotating rate ranging from 400 to 2500 rpm.

In one option, the electron transfer number (n) in an ORR process was calculated by the Koutecky-Levich (K-L) equation:

$$J^{-1} = J_k^{-1} + \left(B\omega^{\frac{1}{2}}\right)^{-1}$$

$$B = 0.62nF(D_0)^{2/3}\nu^{-1/6}C_o$$

$$J_k = nFkC_o$$

where J is the measured current density during ORR, J_k is the kinetic current density, ω is the electrode rotating angular velocity ($\omega = 2\pi N$, N is the linear rotation speed), B is the slope of K-L plots, n represents the electron transfer number per oxygen

molecule, F is the Faraday constant (F = 96485 C mol^{-1}), D_0 is the diffusion coefficient of O_2 in 0.1 M KOH (1.9×10^{-5} cm^2 s^{-1}), ν is the kinetic viscosity (0.01 cm^2 s^{-1}), C_0 is the bulk concentration of O_2 (1.2×10^{-3} mol L^{-1}).

In another option, the electron transfer number (n) and percentage of hydrogen peroxide were quantified by the RRDE measurements, in which the ring potential was constantly set at 1.5 V vs RHE. The HO_2^-% and electron transfer number (n) were determined by the followed equations:

$$n = \frac{4 \times i_d}{i_d + \frac{i_r}{N}}$$

$$HO_2^- \% = \frac{200 \times \frac{i_r}{N}}{i_d + \frac{i_r}{N}}$$

Where n is the electron transfer number, i_d is the disk current, i_r is the ring current and N is the current collection efficiency (0.37) of the Pt ring of the RRDE electrode.

For OER: Electrochemical measurements were performed on an electrochemical station (CHI 760E), with a typical three-electrode system in 1.0 M KOH. The carbon rod and the Ag/AgCl electrodes were used as counter and reference electrode, respectively. The catalyst ink was prepared by the same procedure as the ORR test. For fabricating the working electrodes, 5 μL of the catalyst ink was loaded onto a glassy carbon (GC) electrode of 3 mm in diameter (loading amount was about 0.26 mg cm^{-2}) and then dried at room temperature. Prior to catalyst loading, the GC electrode was carefully polished with 1.0, 0.3 and 0.05 μm alumina powder in sequence, and cleaned by sonication in ethanol and deionized water. Before LSV test, the catalyst was tested for 20 cycles of CV scans to reach a steady state with a scan

rate of 20 mV s^{-1} and a potential range from 1.1 V to 1.8 V (*vs.* RHE). Tafel plots were obtained by linear fitting the plots of overpotentials vs. logarithmic current densities ($\eta = b \log j + a$), and a is the overpotential at current density i = 1mA cm^{-2} and b is the Tafel slope.

The effective electrochemical active surface area **(**ECSA) was estimated from the double layer capacitance (Cdl) of the catalyst surface. The Cdl was determined by measuring CVs at various scan rates within a non-faradaic potential region. The potential range was typically centered at the open circuit potential (OCP) with a potential window of 0.200 V. In this work, CVs were measured in a potential range of 1 V to 1.2 V vs. RHE at different scan rates. The electrochemical double-layer capacitance was determined from the CV curves according to the following equation: $C_{dl} = Ic/\nu$, where C_{dl}, I_c, and ν are the double-layer capacitance (mF cm^{-2}) of the electroactive materials, charging current (mA cm^{-2}), and scan rate (mV s^{-1}), respectively.

7.Zn-air battery performance tests

The measurements of rechargeable zinc-air batteries were performed on home-built electrochemical cells. All data were collected from the as-fabricated cell with a CHI 760D (CH Instruments, Inc., Shanghai, China) electrochemical workstation at room temperature. Briefly, zinc foil was used as anode and the freestanding CoO_x@NC-600 composites cut into 1 cm^2 was directly used as the air cathode. For comparison, the rechargeable battery was also made from a mixture of Pt/C and RuO_2 with a mass ratio of 1:1. The electrolyte in the aqueous batteries was a mixture solution of 6.0 M KOH and 0.2 M zinc acetate.

The all solid-state zinc-air batteries were fabricated by using the polished zinc foil as anode, the freestanding CoO_x@NC-600 composite as cathode, the gel polymer as solid electrolyte, and the carbon cloth as current collector. The solid electrolyte was prepared as follow: 1 g PVA powders (1788-PVA/1799-PVA = 2:1) were added to 10 mL H_2O at room temperature under stirring for 45 min and then heated up to 95 ^oC. After the solution was transformed into transparent gel, 1 mL 18 M KOH was added to the mixture. After being stirred for another 0.5 h, the gel was poured onto a glass plate and frozen in a freezer at -20 ^oC for 2 h. Before used for assembling solid-state ZABs, the gel polymer electrolyte was pre-thawed at room temperature.

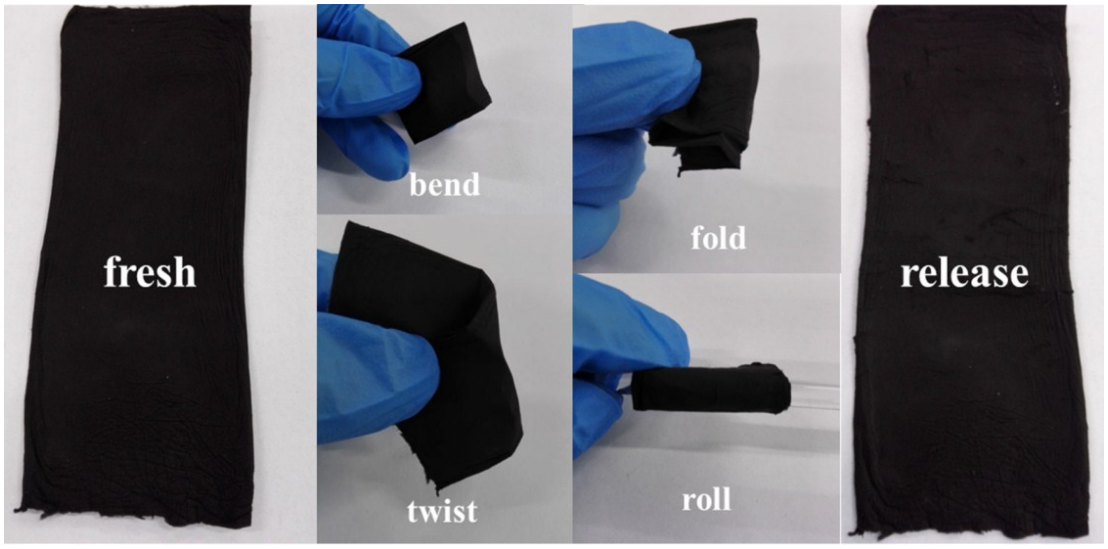

Fig. S1 Digital photographs of flexible CoO_x@NC-600 films showing the deformability and durability of the composite.

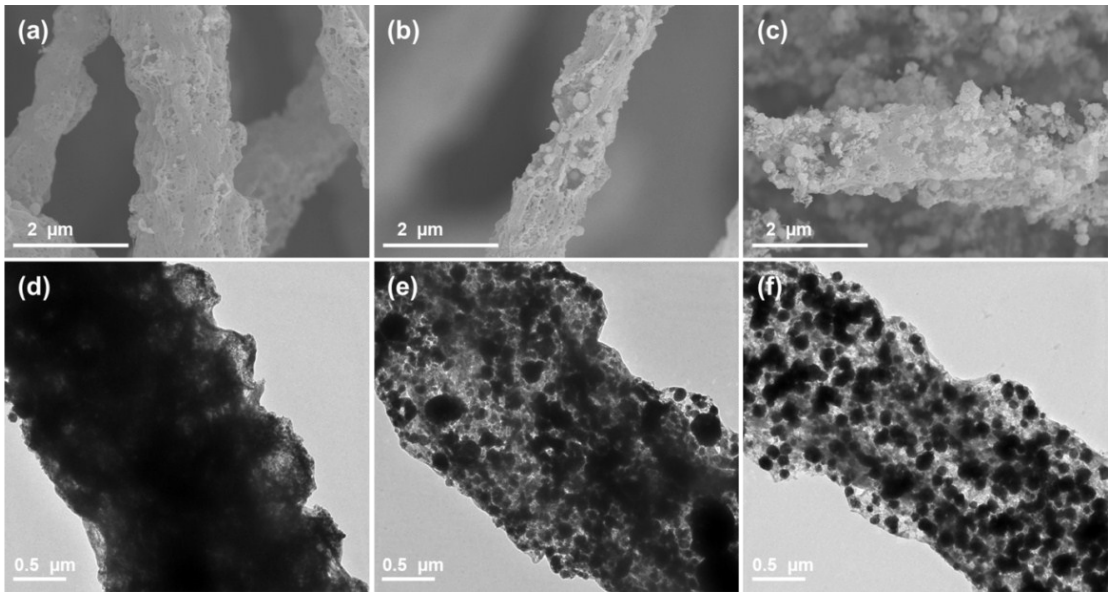

Fig. S2 (a,b,c) SEM and (d,e,f) TEM images of CoO_x@NC-700, CoO_x@NC-800 and CoO_x@NC-900, respectively.

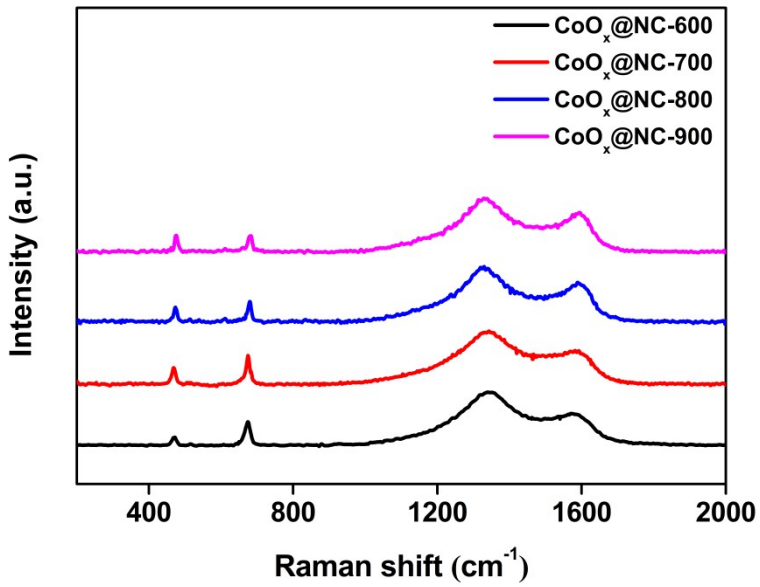

Fig. S3 Raman spectra of the CoO_x@NC composites prepared under various carbonization temperature.

Table S1 Raman peak intensity ratios of CoO/Co_3O_4 and D/G for the CoO_x@NC composites of different carbonization temperature and the calculated x numbers in CoO_x.

sample	Peak intensity ratio (CoO/Co_3O_4)	Peak intensity ratio (D/G)	x*
CoO_x@NC-600	0.34	1.67	1.25
CoO_x@NC-700	0.57	1.58	1.21
CoO_x@NC-800	0.71	1.35	1.19
CoO_x@NC-900	1.03	1.36	1.16

x* is calculated based on the ratio of CoO/Co_3O_4 without considering the trivial amount of Co^0

Table S2 XPS peak intensity ratios of Co^{3+}/Co^{2+}, ICP Co contents, TGA CoO_x contents for the CoO_x@NC composites of different carbonization temperature, and the correspondingly calculated x numbers in CoO_x.

sample	Peak area ratio (Co^{3+}/Co^{2+})	x**	ICP (Co%)	ICP(CoO_x%)	TGA(CoO_x%)
CoO_x@NC-600	1.22	1.27	43	57.8	60
CoO_x@NC-700	0.89	1.23	44	58.7	60
CoO_x@NC-800	0.59	1.18	42	55.4	56
CoO_x@NC-900	0.46	1.15	40	52.4	53

x** is calculated based on the ratio of Co^{3+}/Co^{2+} without considering the trivial amount of Co^0

ICP (CoO_x%) was calculated by the following equation:

ICP (CoO_x%)= ICP (Co%)*(58.93 + 16.00 * x)/58.93

Where ICP (Co%) is the weight percentage of Co measured by ICP and x is calculated from the XPS quantification of Co^{3+}/Co^{2+}.

Table S3 The specific surface area, pore volume and pore size obtained by BET measurements for the CoO_x@NC composites of different carbonization temperature.

Sample	Specific Surface Area ($m^2\ g^{-1}$)	Pore Volume ($cm^3\ g^{-1}$)	Pore Size (nm)
CoO_x@NC-600	240.0	0.21	29.1
CoO_x@NC-700	184.8	0.18	46.7
CoO_x@NC-800	128.7	0.17	55.1
CoO_x@NC-900	50.0	0.07	60.5

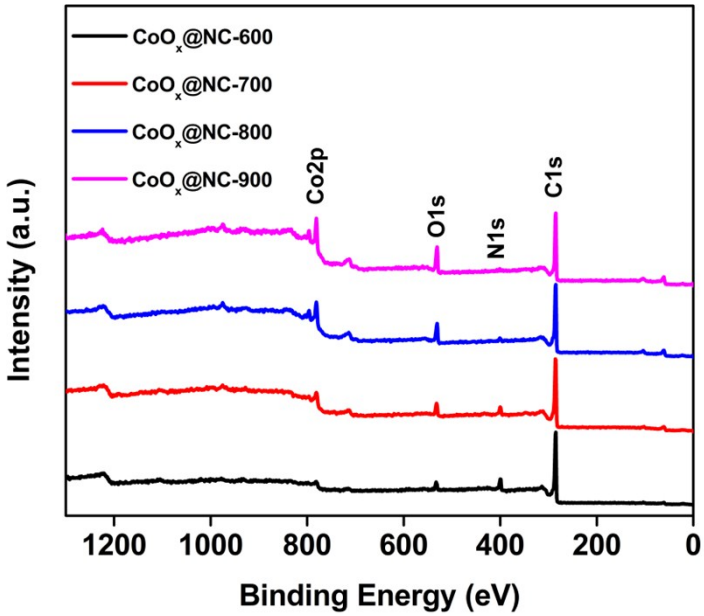

Fig. S4 XPS Survey spectra of CoO$_x$@NC-600, CoO$_x$@NC-700, CoO$_x$@NC-800, and CoO$_x$@NC-900.

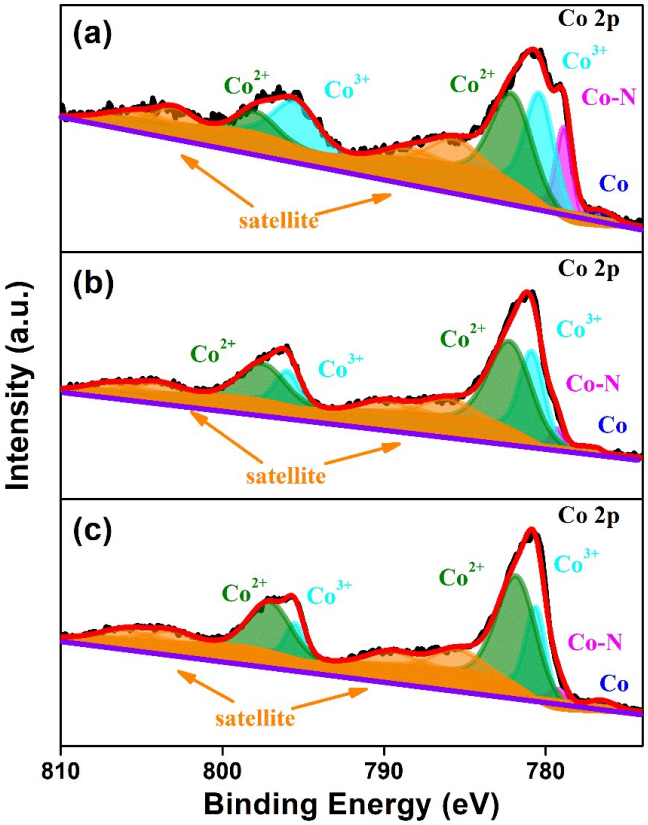

Fig. S5 XPS Co 2p spectra of (a) CoO$_x$@NC-700, (b) CoO$_x$@NC-800, and (c) CoO$_x$@NC-900.

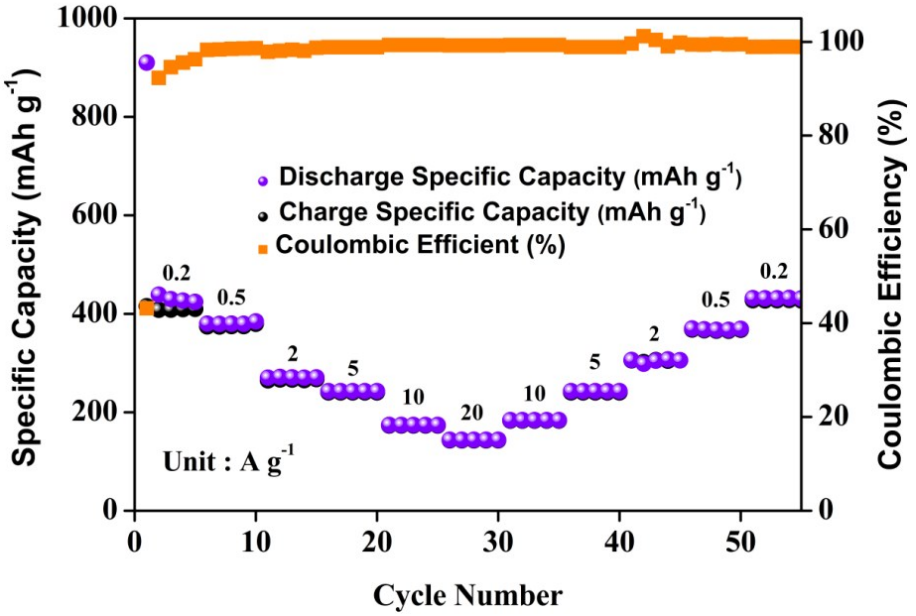

Fig. S6 Rate capability of an SIB half cell with the freestanding CoO_x@NC-600 anode.

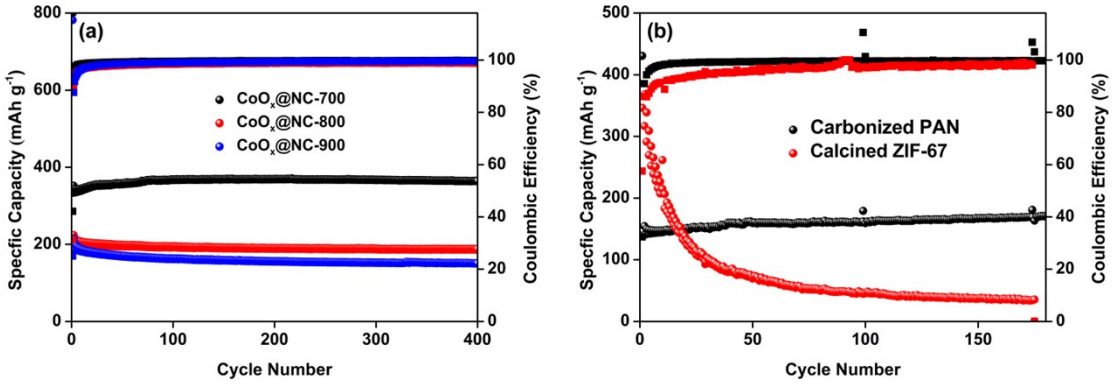

Fig. S7 Cycling performance of (a) CoO_x@NC-700, CoO_x@NC-800 and CoO_x@NC-900; and (b) calcined ZIF-67 and carbonized PAN at the current density of 0.2 A g^{-1}.

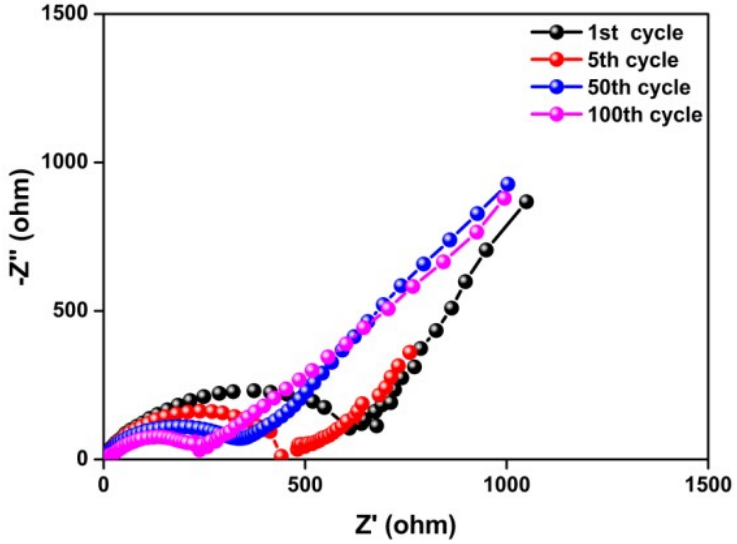

Fig. S8 EIS spectra of the SIB half cell assembled with CoO_x@NC-600 at different cycling status.

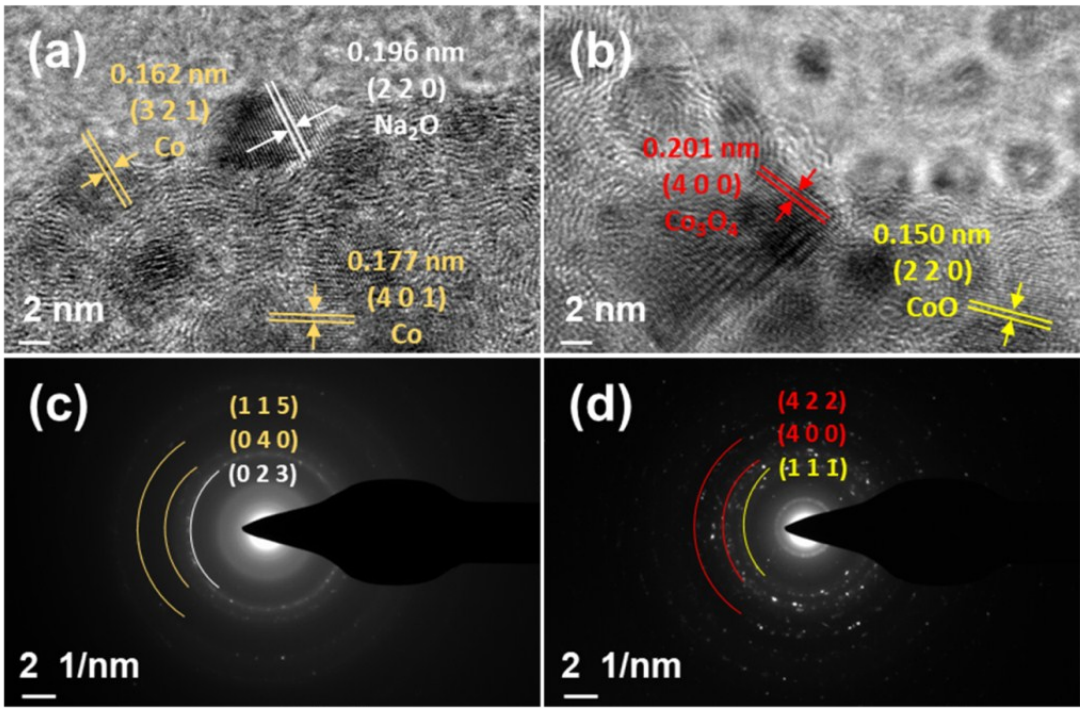

Fig. S9 (a, b) High-magnification view and (c, d) the corresponding SAED images of the CoO_x@NC-600 anodes after fully discharged and charged in SIBs.

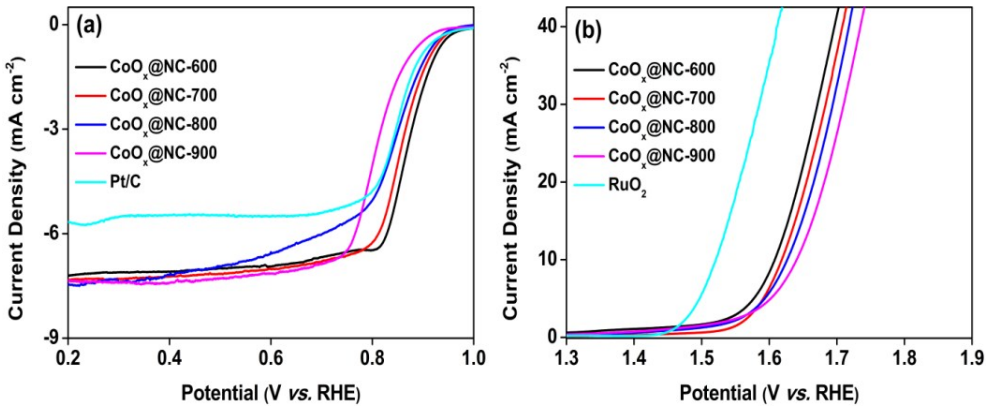

Fig. S10 (a) ORR LSV curves of CoO_x@NC-600, CoO_x@NC-700, CoO_x@NC-800, CoO_x@NC-900 and Pt/C in O_2-saturated 0.1M KOH electrolyte obtained at a scan rate of 10 mV s^{-1} at 1600 rpm; and (b) OER LSV curves of CoO_x@NC-600, CoO_x@NC-700, CoO_x@NC-800, CoO_x@NC-900 and RuO_2 in 1 M KOH electrolyte at a scan rate of 10 mV s^{-1}.

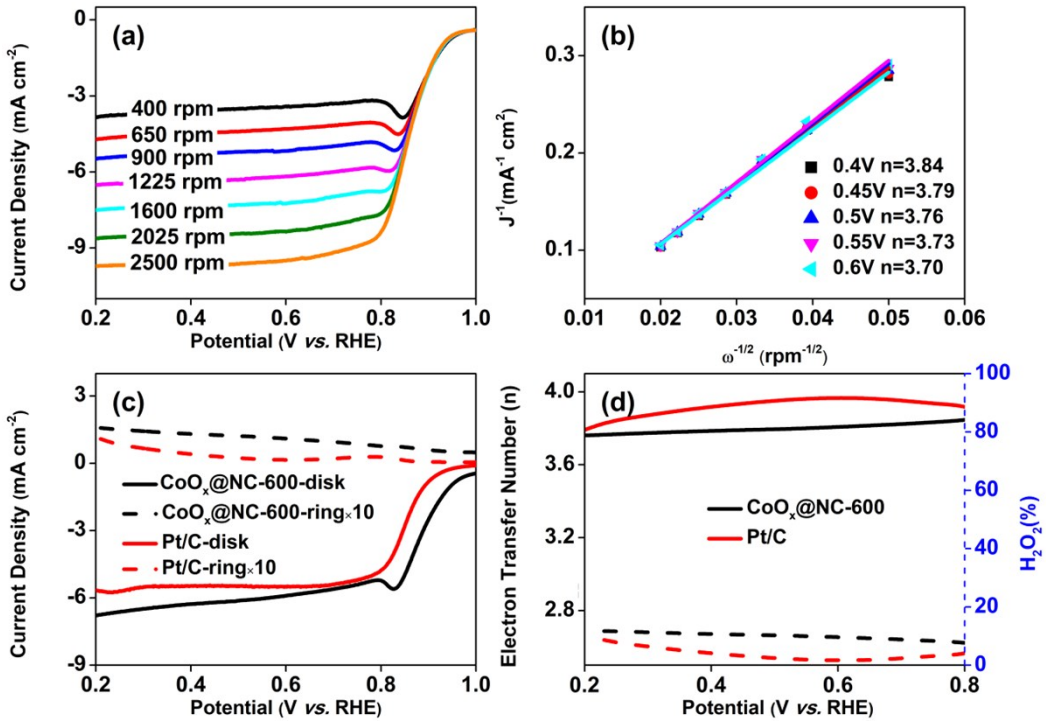

Fig. S11 (a) LSV curves of CoO_x@NC-600 obtained at different RDE rotating rate; (b) the corresponding K-L plots; (c) LSV curves obtained on the rotating ring disk electrode (RRDE) for CoO_x@NC-600 and 20% Pt/C; (d) the plot of electron transfer number and H_2O_2 yield in the potential range from 0.2 to 0.8 V for CoO_x@NC-600 and 20% Pt/C.

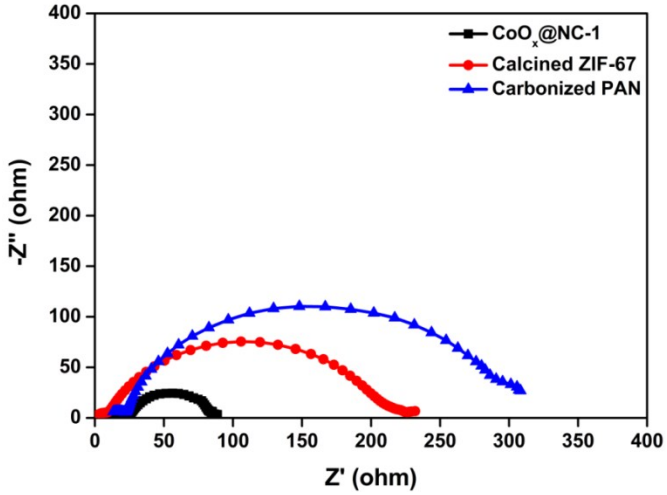

Fig. S12 Nyquist plots of the CoO_x@NC-600, calcined ZIF-67, and carbonized PAN samples acquired during OER at the potential of η_{10}.

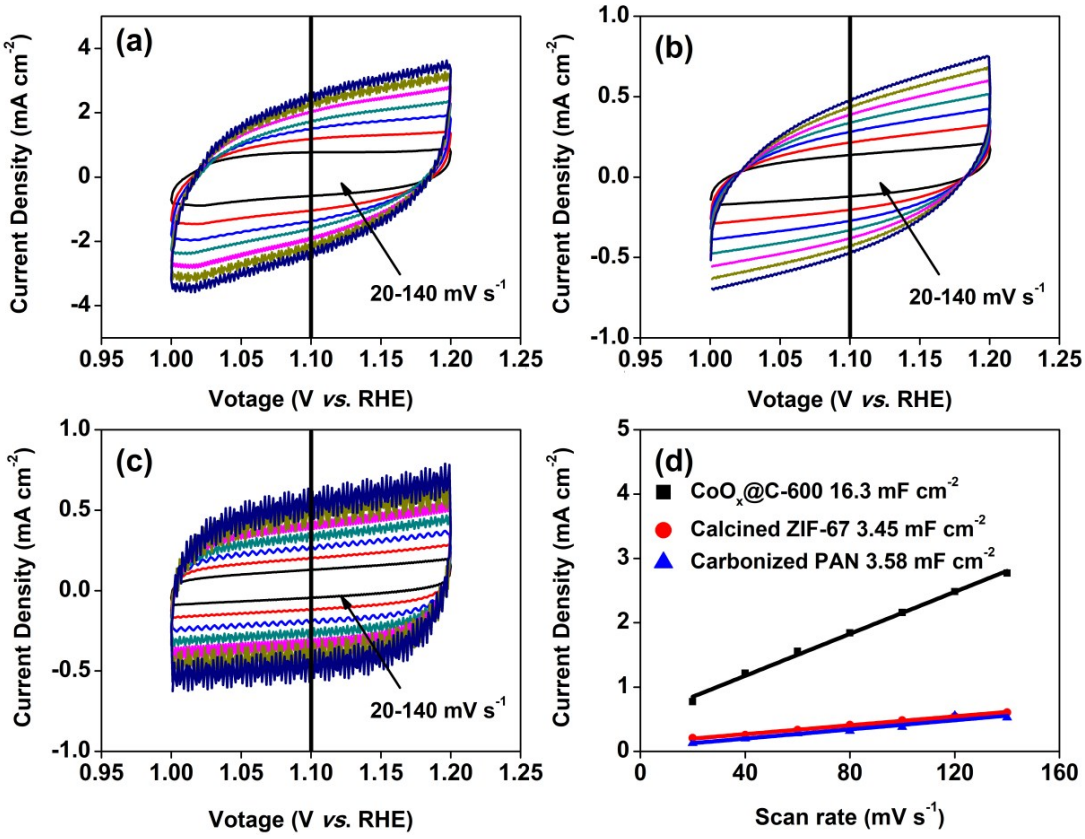

Fig. S13 Rate-varying cyclic voltammetry of (a) CoO_x@NC-600, (b) Calcined ZIF-67, and (c) carbonized PAN for the quantification of double layer capacities (C_{dl}); and (d) plots of the capacitive current densities at 1.10 V (vs. RHE) as a function of scan rate.

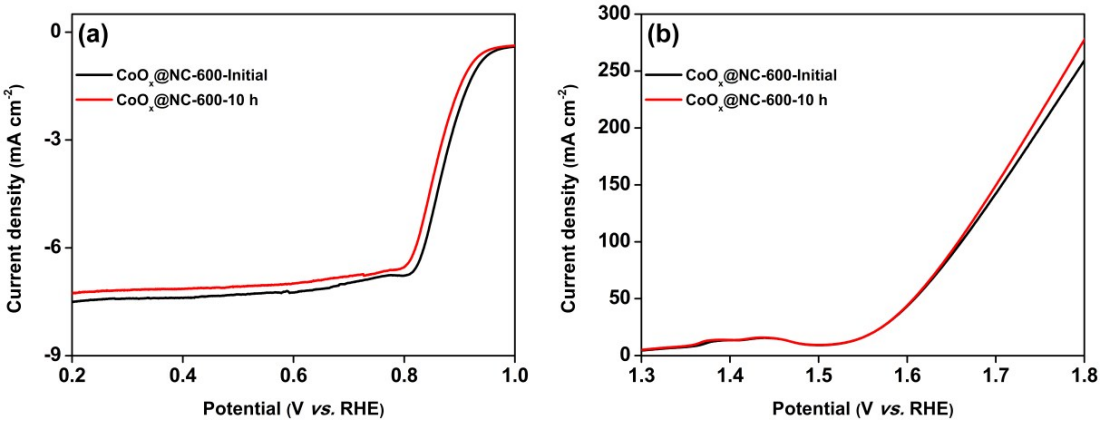

Fig. S14. LSV curves of CoO_x@NC-600 before and after the 10-h chronoamperometric tests for (a) ORR and (b) OER.

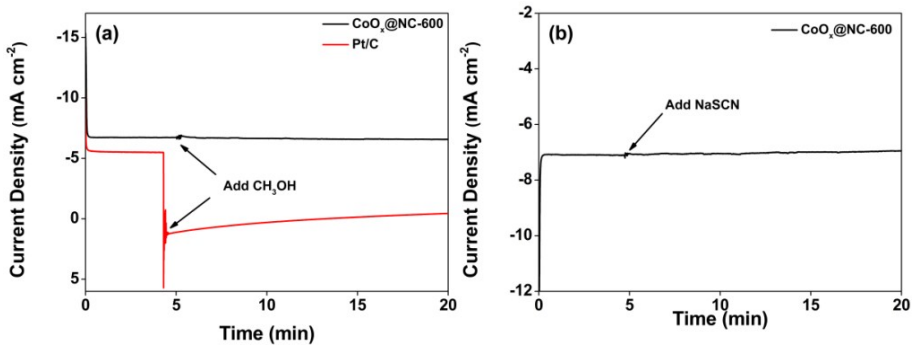

Fig. S15 Chronoamperometric responses of CoO_x@NC-600 and Pt/C after adding (a) methanol and (b) NaSCN.

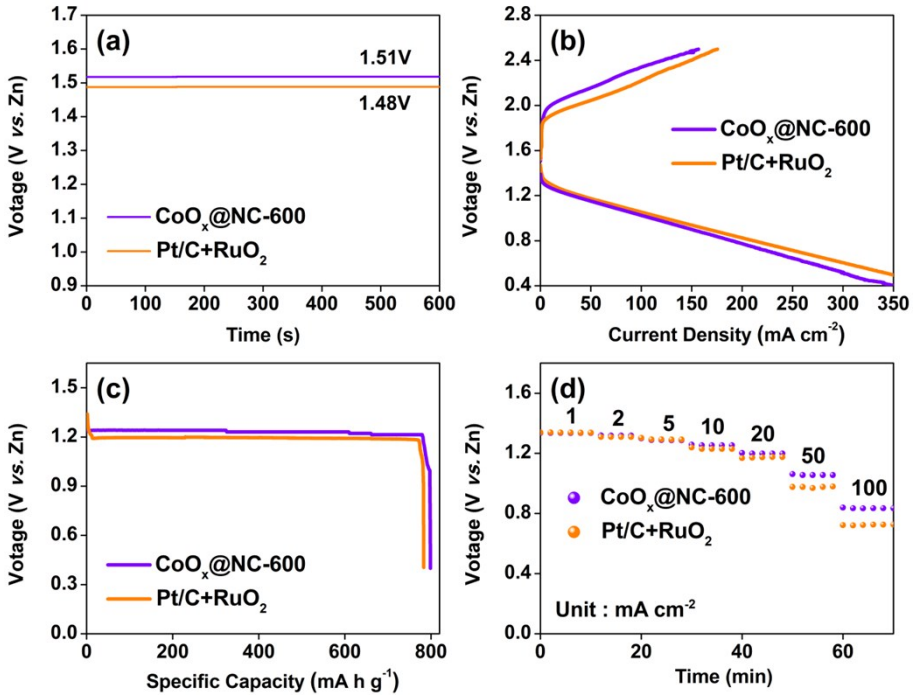

Fig. S16 Electrochemical performances of the aqueous ZABs with CoO_x@NC-600 or Pt/C+RuO_2 as the air cathode catalysts. (a) Plots of open-circuit voltage for ZABs with the CoO_x@NC-600 and Pt/C+RuO_2 air cathode catalysts. (b) ZAB charge and discharge polarization curves for CoO_x@NC-600 and Pt/C+RuO_2; (c) the discharge curves under a constant current of 10 mA cm^{-2} to quantify the specific capacity relative to the consumed Zn mass); (d) plots of discharge voltages at current densities of 1, 2, 5, 10, 20, 50 and 100 mA cm^{-2} for CoO_x@NC-600 and Pt/C+RuO_2 in a total testing period of 70 min.

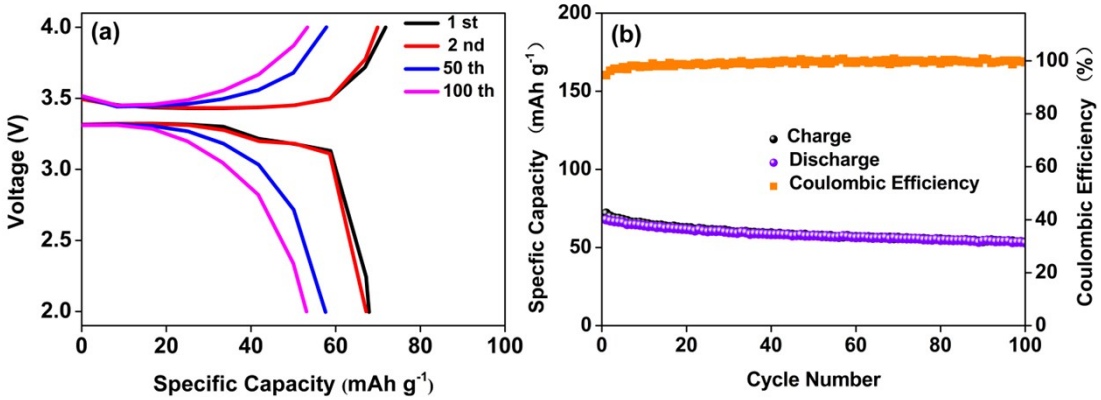

Fig. S17 Sodium storage behaviors of the electrospun $Na_3V_2(PO_4)_3$ cathode ($Na_3V_2(PO_4)_3$@NC-600) vs. metallic Sodium. (a) Charge-discharge curves at different cycles; and (b) cycling performance at a current density of 0.5A g^{-1} for 100 cycles. The results obtained from this test is used to determine the positive/negative ratio in the flexible full cells.

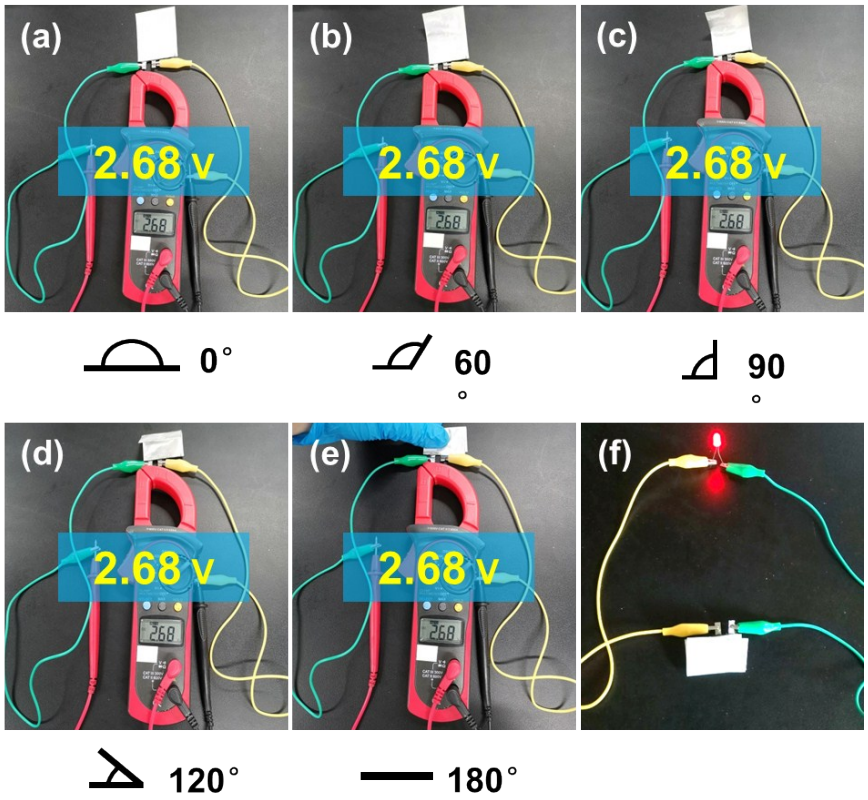

Fig. S18 Digital photos of a flexible SIB full cell showing the open circuit voltages at bending angles of (a) 0^{o}; (b) 60^{o}; (c) 90^{o}; (d)120^{o} and (e) 180^{o}; (f) an LED bulb (voltage input: 1.8 V) constantly lighted by a bent SIB..

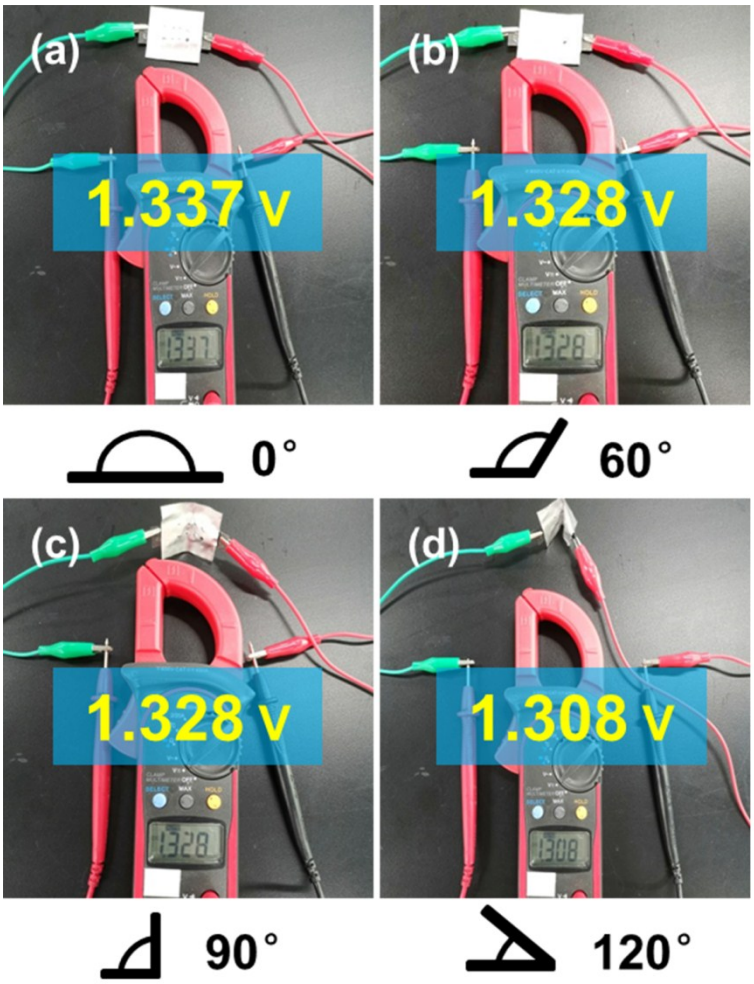

Fig. S19 Digital photos of a flexible ZAB showing the open circuit voltages at bending angles of (a) 0^{o}; (b) 60^{o}; (c) 90^{o}; (d)120^{o}.